ELSEVIER

Biochimica et Biophysica Acta 1186 (1994) 186–200

BBA Biochimica et Biophysica Acta

The effects of calcium depletion on the O_2-evolving complex in spinach PS II: the S_1^*, S_2^* and S_3^* states and the role of the 17 kDa and 23 kDa extrinsic polypeptides

Dugald J. MacLachlan, Jonathan H.A. Nugent *, Peter J. Bratt, Michael C.W. Evans

Department of Biology, Darwin Building, University College London, Gower Street, London WC1E 6BT, UK

Received 25 October 1993; revised manuscript received 16 March 1994

Abstract

Manganese K-edge X-ray spectra have been obtained for Photosystem II samples depleted of calcium by various NaCl treatments which inhibit oxygen evolution without displacement of manganese. Changes in the pre-edge feature due to 1s → 3d transitions and shifts in the edge position of samples in the S_1^*, S_2^* and S_3^* states indicate manganese oxidation for the $S_1^* \rightarrow S_2^*$ and $S_2^* \rightarrow S_3^*$ transitions. Analysis of the EXAFS shows changes on NaCl treatment compared to native PS II membranes which are further modified by the chelator, EGTA. The intensity of the Fourier transform peak at about 1.8 Å, assigned to oxygen, increases with increasing S-state in agreement with oxidation state changes, although the average distance for this first shell remains constant. Each of the inhibitor-treated S-states have a short average Mn–O bond length, showing the retention of the μ-oxo bridges postulated to occur in native samples. The Mn–Mn shell, found at 2.7 Å in native PS II membranes is split in NaCl-treated samples to give a 2.7 Å Mn–Mn and 3.0 Å Mn–X interaction (X = Mn,C/O/N). Splitting of the 2.7 Å shell is most apparent in the higher S-states, $S_3^* > S_2^* > S_1^*$. Although the scatterers at 3.0 Å could not be uniquely identified, the intensity favours heavy scatterers, Mn/Ca, over light scatterers, C/O/N. The cluster appears to contain at least two inequivalent Mn–Mn pairs or shows multiple scattering from a ligand such as tyrosine/histidine. NaCl treatment results in a smaller 3.3/3.6 Å intensity compared to untreated PS II samples which could be due to replacement of calcium scatterers at this distance and/or a structural rearrangement. EGTA addition results in an S_2^* state with a modified EPR spectrum but has only a small effect on the XAS. The changes on removal of the 17 and 23 kDa extrinsic polypeptides are small compared to the effect of the calcium depletion/NaCl treatment, indicating a minor role for these polypeptides on the structure of the cluster. Changes in the electron spin lattice relaxation time, T_1 of the dark stable tyrosine radical $Y_D^{\cdot}$ have also been studied using pulsed EPR. The T_1 relaxation times decreased with increasing modified S-state $S_1^* > S_2^* > S_3^*$, indicating oxidation occurring at or near the manganese cluster.

Key words: Photosystem II; Oxygen-evolving complex; Manganese complex; XANES; EXAFS; Calcium

1. Introduction

Photosynthetic water oxidation is carried out by the membrane-bound pigment-protein complex called Photosystem (PS) II. A manganese-containing complex (oxygen-evolving complex, OEC), located at the membrane lumen interface of PS II, is thought to act as a charge accumulating centre and the catalytic site for water oxidation. The driving force for the generation of oxidising equivalents is the excitation of a reaction centre chlorophyll, P680, which becomes oxidised, the electron passing on to a series of quinones Q_A, Q_B, and a plastoquinone pool. $P680^+$ is reduced by a redox active tyrosine, Y_Z, which in turn oxidises the manganese complex. Removal of four electrons are required for water oxidation resulting in five successive oxidation states, S_i, $i = 0$–4. The highest oxidation state, S_4, oxidises water and spontaneously decays to the S_0 state with the evolution of oxygen, resetting the

Abbreviations: Chl, chlorophyll; DCMU, 3-(3,4 dichlorophenyl)-1,1-dimethylurea; EPR, electron paramagnetic resonance spectroscopy; EXAFS, extended X-ray absorption fine structure; Hpp, peak to trough linewidth of EPR spectrum; MES, 2(*N*-morpholino)ethanesulfonic acid; OEC, oxygen-evolving complex; PPBQ, phenyl-1,4-benzoquinone; PS II, Photosystem 2; S_1^*, S_2^* and S_3^*, modified S states formed in treated samples analagous to native S_1, S_2 and S_3; XANES, X-ray absorption near edge structure; XAS, X-ray absorption spectroscopy.

* Corresponding author. Fax: +44 71 3807096.

SSDI 0005-2728(94)00044-6

cycle. Untreated dark-adapted PS II samples are in the S_1 state. For reviews see [1–4].

PS II is composed of several intrinsic membrane-spanning polypeptides. Two of these, D1 and D2, bind the redox active cofactors necessary for charge separation. PS II also contains extrinsic polypeptides, of apparent mass 17, 23 and 33 kDa, which strongly influence the requirement for the inorganic cofactors. Calcium and chloride are cofactors for physiological function of PS II (see [1,5,6] for reviews). Calcium depletion results in the disruption of electron transfer between the manganese complex and $Y_Z^{\cdot}$, leading to the suggestion that calcium is required for S-state cycling [7–18]. Binding studies on calcium-depleted PS II have identified at least two sites of binding that affect oxygen evolution [11–14].

Electron paramagnetic resonance spectroscopy (EPR) studies of NaCl-washed PS II in the presence of chelators (EDTA, EGTA), or of pH 3 citrate-treated PS II [15–17] have shown a dark stable multiline signal (> 26 lines spread over 160 mT) assigned to the manganese cluster. This EPR signal was removed by addition of calcium with restoration of the oxygen-evolving activity inhibited by these treatments. The dark stable multiline signal was attributed to a chelator modified form of the normal S_2 state multiline, S_2^* ($S' = 1/2$, 18–20 lines spread over 160 mT [19,20]). Measurements of delayed fluorescence yields and the observation of an 13.0–16.0 mT wide split EPR signal (termed S3 signal) following single turnover oxidation of S_2^* [10,15–17,20–22] have identified the inhibition at the $S_3 \rightarrow S_0$ transition.

In order to be able to propose a mode of action for calcium, structural information about the effect of calcium on the manganese complex is necessary. In the absence of an X-ray crystal structure, X-ray absorption studies, XAS, are the only means of obtaining structural data on the manganese complex. The Mn K-edge energy and lineshape is also a sensitive probe of changes in oxidation state and symmetry of the manganese complex. Comparison of K-edge energies with those of model compounds has indicated that in native PS II the states S_1 and S_2 contain predominantly Mn(III) and Mn(IV) [4,23–26]. These studies concluded that the average manganese coordination environment was the same for both states despite a change in oxidation of the manganese and that it contained a short Mn-O/N distance at 1.85 Å, and at least one manganese scatterer at 2.70 Å [25–27]. The Mn-Mn distance and short Mn-O/N distance have been used as evidence for di-μ-oxo bridged manganese pairs as structural elements in the manganese complex [25–27]. Mn K-edge X-ray absorption near edge structure, XANES, spectra of samples 'calcium-depleted' by pH 3 citrate treatment indicate a different conformation and/or an overall lower oxidation state for the manganese cluster in the treated S_1^* samples relative to untreated PS II membranes [28]. Edge measurements of cofactor depleted samples in the S_1^*, S_2^* and S_3^* oxidation states show K-edge shifts between S-states consistent with manganese oxidation on S-state advancement, although structural rearrangements on each of these steps cannot be ruled out [29].

Detergent-treated preparations lacking light-harvesting proteins are also available which are reported to contain only one calcium and retain the extrinsic polypeptides, e.g. [30]. EXAFS of the manganese environment in these preparations show a reduction in the 3.6 Å interaction which was suggested may result from the replacement of calcium by magnesium, a less powerful X-ray scatterer [26].

In addition to Y_Z, another redox active tyrosine, $Y_D^{\cdot}$, is found in the PS II reaction centre D1/D2 complex. Several studies have shown that the electron spin relaxation rate of the radical, $Y_D^{\cdot}$, is influenced by the manganese cluster oxidation state [31–34]. This makes this radical a useful probe of changes in the OEC.

We have investigated the structural and redox changes occurring in the manganese cluster following calcium depletion/NaCl treatment, using EXAFS and EPR techniques. The effect of chelator, EGTA, removal of the 17 and 23 kDa extrinsic polypeptides and the location of calcium sites with respect to the manganese cluster were also addressed and new results obtained.

2. Materials and methods

Spinach thylakoid PS II membranes were prepared from market spinach according to the method of Berthold et al. [35] with the modifications of Ford and Evans [36] (Chl *a*/Chl *b* ratio 2.0–2.20 : 1). These are termed PS II membranes. Reagents used were all analytical grade. Both the 2(*N*-morpholino)ethanesulfonic acid, MES, and sucrose solutions were treated with Chelex before use. All laboratory ware was washed with 0.1 M HCl and rinsed with Chelex treated double distilled water before use.

Calcium depletion was achieved in three ways resulting in sample types termed (1) calcium-depleted plus polypeptides (containing all extrinsic polypeptides), (2) calcium-depleted minus polypeptides (lacking 17 kDa and 23 kDa polypeptides but retaining the 33 kDa polypeptide), and (3) NaCl-treated (lacking 17 kDa and 23 kDa polypeptides but retaining the 33 kDa polypeptide).

(1) Prepared by a method based on Boussac et al. [15] which results in a dark stable multiline signal on illumination at 0–4°C and the reconstitution of the 17 and 23 kDa extrinsic polypeptides. PS II membranes were first washed in 0.3 M sucrose, 10 mM NaCl, 25

mM MES, 2 mM EGTA (pH 6.5) (Buffer A). Calcium depletion was carried out by treatment with 0.3 M sucrose, 1.2 M NaCl, 20 mM MES, 50 μM phenyl-1,4-benzoquinone, PPBQ, 20 mM EGTA (pH 6.5) at 5 mg Chl/ml and rapidly transferred to a 8–10 kDa cutoff dialysis membrane. Dialysis was carried out for 2 h under room light at 4°C against 2 l of 0.3 M sucrose, 20 mM MES, 1.2 M NaCl (pH 6.5) and then for 3 h in the dark against 0.3 M sucrose, 20 mM MES (pH 6.5). The membranes were isolated by centrifugation (40 000 $\times g$, 15 min) and the pellet resuspended in a buffer containing 50 mM NaCl, 20 mM MES, 5 mM EGTA (pH 6.5).

(2) Prepared by a method based on Boussac et al. [20] which does not reconstitute the 17 and 23 kDa extrinsic polypeptides. PS II membranes were first washed in Buffer A. The membranes were treated with a buffer of 1.2 M NaCl, 25 mM MES, 0.3 M sucrose, 50 μM PPBQ (pH 6.5) at 0.5 mg Chl/ml under room light for 30 min. After this time EGTA was added to a final concentration of 50 μM and the membranes isolated by centrifugation (40 000 $\times g$, 15 min). The pellet was resuspended in a buffer containing 50 mM NaCl, 25 mM MES, 20% glycerol (pH 6.5).

(3) 'NaCl-treated' PS II samples were prepared [29,37] by first washing PS II membranes with 40 mM MES, 25 mM NaCl (pH 6.0) in order to adjust the pH and remove divalent cations present in the storage buffer. The isolated PS II membranes were resuspended in 0.3 M sucrose, 40 mM MES, 600 mM NaCl, 1 mM PPBQ (pH 6.0). When 5 mM EGTA was added to the final buffer the samples are termed 'NaCl-EGTA treated'. Centrifugation of the preparation at 40 000 $\times g$ for 30 min, followed by SDS polyacrylamide gel electrophoresis of the pelleted material showed that the 17 and 23 kDa extrinsic polypeptides but not the 33 kDa polypeptide are released by the high salt concentrations (600 mM) as expected (see [1–3] for reviews of the effects of high salt concentrations).

The simple high salt procedure 3 was introduced because it enabled a better comparison between different salt treatments, simplified sample preparation without a significant change in properties and minimised exposure to light ensuring retention of a S_1^* state. Dialysis of the treated samples to reduce the salt concentration as in the calcium depletion procedure given in method 1 gave samples with identical EPR and very similar oxygen evolution properties. It was, however, difficult during dialysis and centrifugation (a) to eliminate exposure to light, allowing formation of dark stable S_2^* (detected by EPR) in significant amounts and (b) to obtain samples free of contaminating Mn^{2+}.

The membranes obtained and used as a result of the calcium depletion treatments were depleted of greater than 90% of their oxygen-evolving activity. This was measured in a Clark-type oxygen electrode at 298 K using ferricyanide and PPBQ as electron acceptors. The control was depleted membranes to which 20 mM calcium chloride was added and then incubated for 30 min at 277 K in the light. Control rates of oxygen evolution for PS II membranes were 300–600 μmol O_2/mg Chl per h dependent on the particular batch of PS II membranes used.

2.1. Preparation of samples in different S-states

All procedures were carried out in the dark or under a dim green light, producing samples initially in the S_1^* state, as indicated by the absence of a multiline EPR signal. S_1^* samples were then frozen in the dark. To obtain the S3 EPR signal, samples were illuminated on each side at 277 K for 1 min (total 2 min) using an unfiltered 650 W light source (1000 $\mu E/m^2/s$) and then frozen rapidly to 77 K in the dark or under illumination. Samples formed by this procedure contain $< 15\%$ of the maximum S_2^* multiline intensity. S_2^* was generated by initially illuminating as for the S3 EPR signal, then storing the sample at 273 K for 5 or 10 min in the dark to allow relaxation to S_2^*, before freezing to 77 K. In the case of NaCl-treated samples, the amount of S_2^* multiline EPR signal formed was $> 90\%$ that of a sample containing 0.5 mM 3-(3,4 dichlorophenyl)-1,1-dimethylurea, DCMU, that was illuminated directly from S_1^* to S_2^*. Illumination treatments for EPR and EXAFS samples were carried out immediately before measurement. Light limitation was unlikely to occur in the illumination regimes employed. However, samples of identical concentration were checked by EPR to ensure that illumination produced identical changes in modified S-state in both EPR and EXAFS.

2.2. EPR spectrometry

For EPR at cryogenic temperatures, 0.3 ml samples (at approximately 10 mg Chl/ml) were placed in calibrated 3 mm diameter quartz EPR tubes. Samples for EPR, made in parallel with the EXAFS samples from the material remaining after EXAFS sample preparation as given in [29], were resuspended and loaded into EPR tubes or samples at EXAFS concentration (> 50 mg Chl/ml) were made using specially adapted holders. During dark adaptation, samples were kept on ice at 273 K. Using the signals present in control samples (cytochrome *b*-559 etc.,) the EPR spectrometer and measurement conditions were calibrated for experiments which involved EPR data collection on different days. EPR spectrometry was performed using a Jeol RE1X spectrometer fitted with an Oxford Instruments liquid helium cryostat. EPR conditions are given in the figure legends. Spectra were recorded and manipulated using a Dell microcomputer running Asyst software. The vertical scale in figures showing first derivative

EPR spectra is arbitrary, with spectra at the same instrument gain unless stated in the figure legend.

2.3. EXAFS

EXAFS samples were prepared by centrifugation at $260\,000 \times g$ for 1 h and then loaded into polycarbonate EXAFS holders. None of the samples (lacking EGTA) contained significant amounts of Mn^{2+} as indicated by the absence or near absence of a Mn^{2+} six line EPR spectrum. The maximum contamination by Mn^{2+}, estimated by comparison to a 2 M HCl-treated sample, was $\ll 5\%$. For EGTA containing samples it is not possible to determine free Mn^{2+} using EPR as the addition of EGTA renders such species EPR silent.

Ideally EPR and EXAFS measurements should be done on the same sample with EPR being carried out immediately before and after EXAFS measurements. Facilities for EPR at cryogenic temperature are not available at Daresbury, therefore EXAFS and EPR samples were made for each treatment from the same preparation. Making the EPR samples immediately after the EXAFS samples ensured any sample deterioration was noted. EPR samples were also taken from the EXAFS sample following EXAFS measurements. This procedure provided monitoring of EXAFS sample condition and avoided problems of decay of higher S-states that might have occurred between EXAFS and EPR measurements on the same samples. The S-states were characterised by EPR measurements monitoring the S_2 multiline signal and the S3 EPR signal [29]. Very similar yields of EPR signal (using cytochrome *b*-559 as a control) were seen from different preparations of each treatment. Addition of 20 mM calcium chloride to dialysed samples followed by 30 min incubation in the light restored the normal S-state turnover and S_2 multiline formation.

EXAFS measurements were detected in the fluorescence mode at the Synchrotron Radiation Source at the SERC Daresbury Laboratory [26]. All the samples were measured on beamline 8.1 with a slitless Si(220) double crystal monochromator. Detection of the fluorescence was with a thirteen element Ge solid-state detector windowed on a 5 mM $MnCl_2$ solution. Spectra were recorded at 77 K with a beam energy of 2 GeV and an average beam current of 160 mA. Five scans, each lasting appoximately 1 h, were accumulated per sample. To maintain samples fully in S_3^*, samples were illuminated for 30 s in the EXAFS cryostat after two scans. No photoreduction of the samples was observed during the data collection, confirmed by examining edge positions for each scan before averaging. Data reduction was as described [26]. Energy calibration was based on the pre-edge peak of $KMnO_4$, 6543.3 eV, and confirmed with the first inflection of the edge for Mn foil, 5 μm, 6538.0 eV. Individual detector elements of each scan were examined separately for anomalies and weighted by the edge-jump before averaging and energy calibration with the Daresbury EXCALIB program. The averaged spectra were normalised to an edge jump of one and the EXAFS were extracted by removing the background absorption using the Daresbury EXBACK program. Normalized background subtracted data are presented in k-space, where k is the photoelectron wave vector defined by $[2m_e(E - E_0)/\hbar]$, m_e is the electron mass, E_0 is the photoelectron energy zero taken as the edge energy and $\hbar$ is Planck's constant divided by 2π. The EXAFS were weighted by k^3 and analyzed using EXCURV92, which calculates the theoretical EXAFS using the fast curved wave approach [38]. The fits to the Fourier transforms of the experimental data used the non-linear least-squares minimisation program. Phase shifts were calculated by ab initio methods within the EXCURV90 program and verified with model compounds [26]. Differences between crystallographic distances and theory ranged between 0.00 Å and -0.04 Å. Analysis of model compounds gave an amplitude reduction factor for multielectron absorption of 0.7, while the imaginary part of the photoelectron self-energy was set to -1 eV in order to reproduce the elastic electron mean free path. The photoelectron energy zero, E_0, was treated as a single overall parameter in the multiple-shell fits. E_0 refined to values close to those obtained for model compounds, 20–30 eV, below the experimental absorption threshold. For all of the PS II samples, E_0, refines to a value between 25–27 eV, which is similar to that found in our earlier study on PS II membranes [26]. The Fourier transforms were calculated with the plane wave approximation and corrected for the phase shift of the first shell of backscattering atoms resulting in peaks at approximately the expected radial distance [39]. Data analysis was performed on the raw EXAFS in k space, k^3-weighted, with use of the Fourier transform confined to model building and visual determination of quality of fit. In the fitting tables we show the following statistical criteria as recommended by the International Workshop on Standards in EXAFS. Structural models were compared by comparing the fit index, FI, defined as

$$\sum_i^N 1/\sigma_i^2\{\chi^{\exp}(k_i) - \chi^{\text{the}}(k_i)\}^2$$

where $1/\sigma_i = k_i^n/\sum_j^N k^n \mid \chi^{\exp}(k_j)\mid$, N is the number of data points, n is selected to produce a constant envelope amplitude for $k^n\chi^{\exp}(k)$ ($n = 3$ for k^3 weighted data), the sum of which is the experimental amplitude of the spectra and is a constant, and the agreement factor, R; defined as $\sum_i^N 1/\sigma_i\{\mid \chi^{\exp}(k_i) - \chi^{\text{the}}(k_i)\mid\}100\%$.

Use was also made of an absolute index of goodness of fit, given by the reduced χ^2 function:

$$\epsilon_v^2 = 1/N_{\text{ind}} - p(N_{\text{ind}}/N) \sum_i^N 1/\sigma_i^2 \{\chi^{\text{exp}}(k_i) - \chi^{\text{the}}(k_i)\}^2$$

where N_{ind} is the number of independent points, $N_{\text{ind}} = 2(r_{\max} - r_{\min})(k_{\max} - k_{\min})/\pi$ and p is the number of parameters.

For fitting purposes the only light atoms coordinated to the manganese were considered to be oxygens. This is consistent with current evidence which suggests only a small number of nitrogen ligands [1–4,40]. We adopted a fitting procedure whereby the coordination numbers were varied systematically in steps of 1.0 while the Debye-Waller factors, $2\sigma^2$ where σ is the root mean square deviation in the interatomic distance, were refined to obtain the best simulation. The Debye-Waller factors reflect the thermal and static disorder in the bond distances. Coordination numbers and Debye-Waller factors were refined together using different initial values for these parameters. From these calculations the errors associated with the coordination numbers are $\pm 20\%$ for the short oxygen and manganese shells and ± 30–50% for the longer oxygen shell. The estimated error for the radii are $\leq 2\%$ and for the Debye-Waller factors ± 30–50%.

2.4. Pulsed EPR

Relaxation transients were measured using a Bruker ESP380E X-band pulsed spectrometer operating near 9.74 GHz, equipped with a variable Q, dielectric resonator, Bruker model 1052 DLQ-H 8907. The sample was maintained near 4 K by an Oxford Instruments CF935 flowing gas cryostat. For a 16 ns pulse in a $S = 1/2$, $g_e = 2.002$ system, the maximum microwave magnetic field generated by a 1 kW travelling wave tube amplifier was approximately 6 G within the 10 mm homogeneous region of the resonator. All measurements were accumulated with a cavity Q of about 100 resulting in a minimum deadtime of approx. 100 ns. The 90° pulse width was 16 ns and the echo was detected with a sampling digitizer.

Spin lattice relaxation times were recorded by two methods. The first method was that of repetition rate saturation and utilised the following pulse sequence

$$[(\pi/2\text{-}T\text{-}\pi\text{-}T\text{-}Echo)_n\text{-}\tau\text{-}(\pi/2\text{-}T\text{-}\pi\text{-}T\text{-}Echo)_n \ldots]$$

where saturation is achieved by making the repetition rate, (τ) initially very short, and then sequentially incrementing τ until the maximum echo intensity is achieved. In order to set up a steady state three dummy cycles were used but not recorded. The maximum repetition rate was 1000 Hz, and the spin echo interpulse delay, T, was 112 ns.

The second method employed to determine spin lattice relaxation times was that of saturation recovery utilising the following pulse sequence:

$$[P1\text{-}\tau\text{-}(\pi/2\text{-}T\text{-}\pi\text{-}T\text{-}Echo)]_n$$

where P1 is a pulse of sufficiently long duration to saturate the energy level transition of the signal of interest. The value of P1 used was typically 2000 ns. The progress of the bulk magnetization back to equilibrium was detected by the Hahn spin echo sequence after a variable time, τ. As before the value of T was 112 ns. Measurements of the relaxation transients were made at five different fields spaced at centre field for the signal, 5 and 10 G each side of centre field. This was necessary to eliminate any contribution to the relaxation transients from other $g = 2$ radicals that might form under the sample preparation conditions. The relaxation transients were fitted using both proprietary Bruker software which allows for the fitting of multiple exponentials to the decay curves and software written by the authors.

3. Results

3.1. EPR

The EPR properties of the calcium-depleted preparations plus or minus the 17 and 23 kDa polypeptides have been reported previously [10,15,17,20]. With both calcium-depleted samples (± 17 and 23 kDa polypeptides) the S_1^* state was prepared using long term (> 4 h) dark adaptation. As a result of illumination during early steps of the preparative procedure some dark stable S_2^* was formed as monitored by EPR of the multiline signal. A long dark adaptation lead to release of some manganese as Mn^{2+}, while shorter dark adaptation did not result in a complete decay of the S_2^* multiline EPR signal. As the 'NaCl-treated' samples were prepared in the dark, unilluminated NaCl-treated samples are in the S_1^* state and do not exhibit any EPR signals attributable to the manganese cluster. Removal and reconstitution of the 17 and 23 kDa extrinsic polypeptides were established by SDS-polyacrylamide gel electrophoresis and confirmed by the EPR characteristics of the samples, i.e. the splitting obtained for the S3 signal generated by freezing under illumination was approximately 16 mT for reconstituted samples and approximately 13 mT for the samples which lack the two extrinsic polypeptides [15,20].

Fig. 1 shows the EPR spectra of the NaCl-treated preparation in the S_1^* and S_2^* states. As calcium depletion blocks S-state transitions past S_3, the S_3^* state can be accumulated by illumination at 273 K followed by freezing to 77 K with continuing illumination, Fig. 2. An EPR signal is generated, which we term the S3

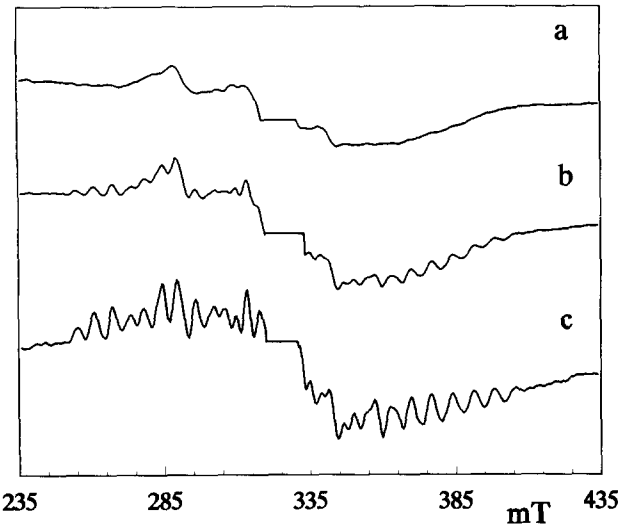

Fig. 1. EPR spectra of NaCl-treated PS II membranes. (a) Dark-adapted sample. (b) Sample containing 5 mM EGTA after 1 min of 277 K illumination followed by dark adaption for 5 min before freezing. (c) Difference spectrum at higher instrument gain of spectrum b with spectrum of a dark-adapted sample before illumination subtracted. Spectrometer conditions: microwave power 5 mW, modulation amplitude 2 mT, temperature 9 K. The central $g = 2$ region has been erased to remove the $Y_D^{\cdot}$ radical. The signal at 290 mT is due to cytochrome *b*-559.

signal, although its origin is not fully understood. The S_2^* multiline signal is small or absent in these samples. The S3 EPR signal showed splitting of about 16 mT both in the presence and absence of chelator, which is in the range observed for calcium-depleted samples in other studies, with or without the 17 and 23 kDa extrinsic polypeptides [15,20]. In calcium-depleted samples the S_2^* state is stabilised, so that the dark relaxation of an illuminated S_3^* state sample results in charge recombination ($t_{1/2} < 30$ s), allowing the trapping of the S_2^* state in good yield. When the NaCl-treated sample contained EGTA, a dark stable multiline EPR signal was obtained in the S_2^* state, Fig. 1c. In these samples the signal comprises at least 26 lines separated by ≈ 55 G and the signal was removed following addition of calcium and dark incubation. The change in the multiline splitting could arise for example from changes in the bond angles of the bridging ligands, protonation of a μ-oxo ligand or a change in the number of bridging ligands in a manganese dimer. Samples without EGTA did not exhibit a prominent multiline EPR signal, indicating decay of the S_2^* state on thawing the sample or the formation of an EPR silent oxidation state. Samples in S_1^* do not advance to S_3^* if the reaction centre is restricted to a single turnover by addition of 0.5 mM DCMU before illumination at 273 K but the dark stable multiline is formed in samples containing EGTA [10]. These characteristics confirm the very similar EPR properties of NaCl-treated PS II to that seen after calcium depletion by other groups [15,17,20].

3.2. XANES

Structural and conformational changes to the manganese cluster are observable by XAS. Changes in oxidation state and symmetry of the manganese cluster are most readily detected in the pre-edge and XANES regions which extend about 20 eV before and 50–100 eV after the absorption edge. The Mn K-edge positions of the NaCl-treated samples are tabulated in [29].

The Mn K-edged spectra of all the calcium-depleted S_1^* samples appeared to be very similar, as were the edge positions, measured as 6550.5–6551 eV relative to Mn foil (6538.0 eV) and $KMnO_4$ (6543.3 eV). Removal or reconstitution of the two extrinsic polypeptides from the calcium-depleted samples does not cause a discernable effect at the current level of signal to noise. The addition of chelator to the calcium-depleted samples (± 17 and 23 kDa polypeptides) does not cause an effect on the edge position within the limits of experimental accuracy, indicating the same overall oxidation states for samples prepared with and without EGTA. That all the samples have very similar edge positions argues against significant free Mn^{2+} being present.

Comparison of the XANES region from different samples can be obtained by using second derivatives to emphasize features on the absorption edge. However, complete interpretation of the edge region would require greater knowledge of the structure of the manganese complex and ligands than is presently available. The pre-edge feature near 6540 eV is assigned to a semiforbidden 1s → 3d quadrupole transition which de-

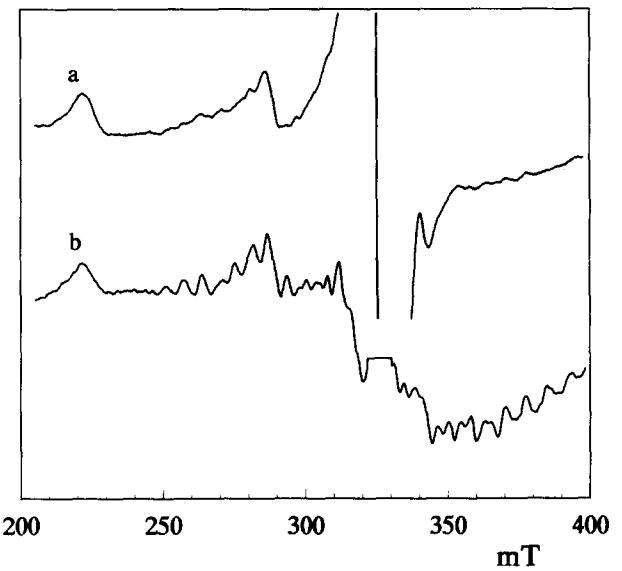

Fig. 2. EPR spectra of NaCl-EGTA-treated PS II membranes, showing the loss of the dark stable multiline S_2^* and appearance of the S3 EPR signal following 277 K illumination. (a) Sample frozen to 77 K during illumination following 1 min illumination at 277 K. (b) Sample thawed and refrozen after 5 min dark adaptation at 277 K. Spectrometer conditions as Fig. 1.

rives intensity from vibronic coupling and p – d orbital mixing. On the rising edge of the main absorption are a series of features thought to be due to 1s → 4p and 1s → 4p + metal ligand charge transfer shakedown transitions. Second derivatives of the edge region showed features similar to those reported for samples 'calcium-depleted' by pH 3 citrate treatment [4], Figs. 3 and 4. The differences between the untreated and treated PS II samples could be explained by oxidation state changes of particular atoms of the complex, e.g. a redistribution of charge in S_1. In [29] where absorption edge measurements are discussed in detail, we interpreted changes in the edge positions for different treatments as conformational changes where samples were in the same S-state. The changes in the pre-edge feature support a conformational change between untreated and NaCl-treated or calcium-depleted samples in the S_1^* state. Binding of the 17 and 23 kDa polypeptides does not seem to affect the Mn K-edge energy or significantly alter its shape, implying the effect of the extrinsic polypeptides is subtle. Small differences also occurred between samples to which EGTA had been added and those without indicating some structural differences induced by EGTA, as indicated by EPR studies. The greatest differences between samples were for the different S-states, Fig. 4. The largest change observed was for the $S_2^* \rightarrow S_3^*$ transition, which results in sharper, more intense pre-edge and better defined edge features.

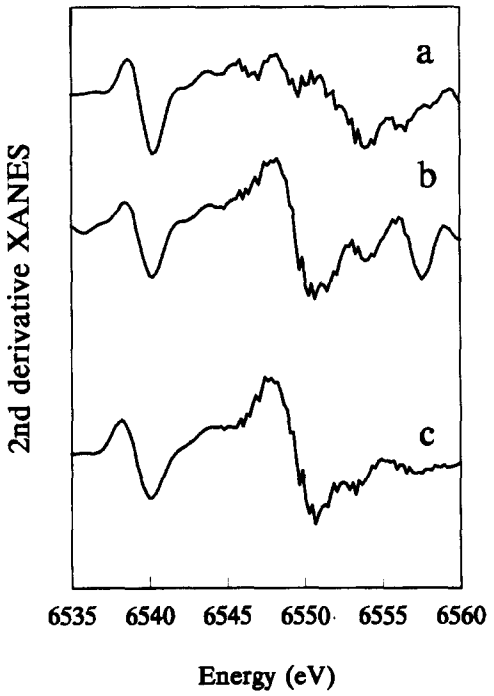

Fig. 3. Second derivative of the Mn K-edge XANES region for (a) PS II membranes in S_1, (b) calcium-depleted PS II membranes minus the 17 and 23 kDa extrinsic polypeptides in S_1^*, (c) calcium-depleted PS II membranes reconstituted with extrinsic polypeptides in S_1^*. The spectra were smoothed with a ninth order polynomial smoothing function before differentiation.

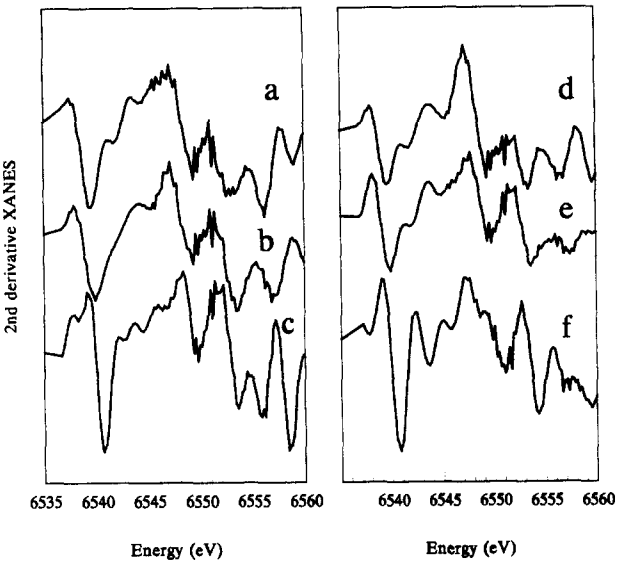

Fig. 4. Second derivative of the Mn K-edge XANES region. (a), (b) and (c) are NaCl-treated PS II samples with the S_1^*, S_2^* and S_3^* states formed as given in Section 2. (d), (e) and (f) are for the S_1^*, S_2^* and S_3^* states of NaCl-EGTA treated samples. Other conditions as given in Fig. 4 and Section 2.

3.3. EXAFS

Figs. 5 and 6 show examples of the raw k^3-weighted EXAFS data (5A, 6A) and Fourier transforms (5B, 6B) for six samples; 600 mM NaCl-treated samples in the S_1^*, S_2^* and S_3^* states with and without chelator, EGTA, added. The untreated S_1 state in PS II membranes is shown for comparison in each case. Samples treated

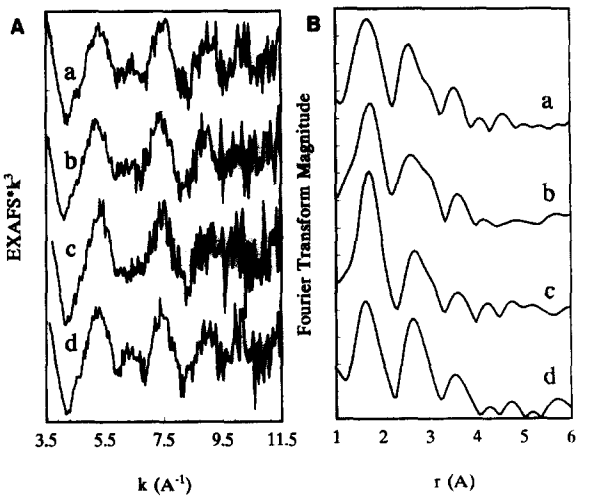

Fig. 5. Raw EXAFS k^3-weighted (A) and Fourier transforms k^3-weighted (B) for NaCl-treated PS II samples in the (a) S_1^*, (b) S_2^* and (c) S_3^* states. Sample (d) is of untreated PS II membranes in the S_1 state. Other conditions as given in Section 2.

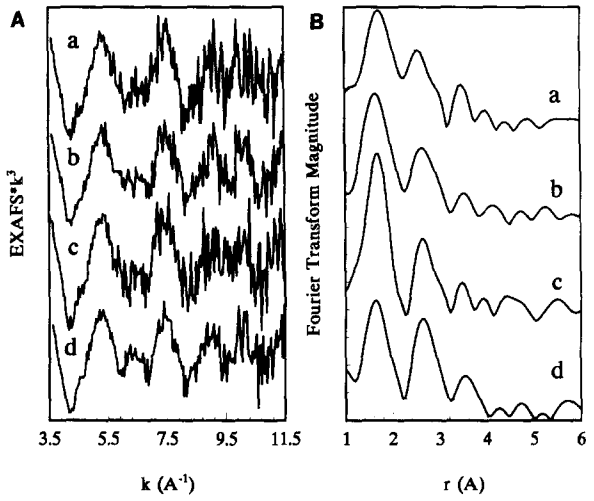

Fig. 6. Raw EXAFS k^3-weighted (A) and Fourier transforms k^3-weighted (B) for NaCl-EGTA treated samples in the (a) S_1^*, (b) S_2^* and (c) S_3^* states. Sample (d) is of untreated PS II membranes in the S_1 state. Other conditions as given in Section 2.

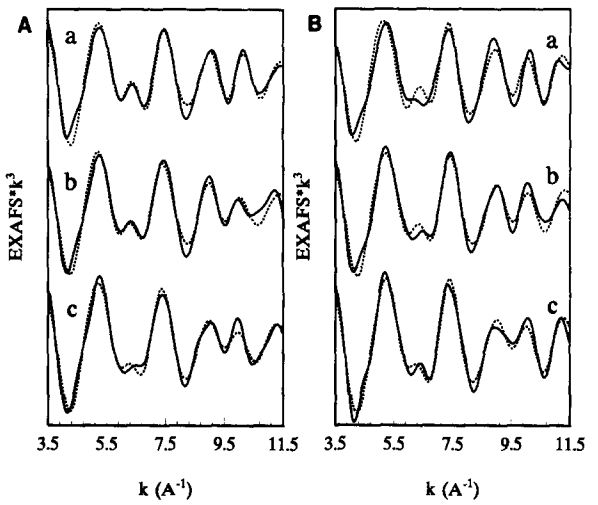

Fig. 7. Three shell fits to the Fourier filtered k^3-weighted EXAFS data of (A) NaCl-treated samples and (B) NaCl-EGTA treated samples. Samples were in the (a) S_1^*, (b) S_2^* and (c) S_3^* states. The Fourier filter window was 0.7–4.5 Å, uncorrected for phase. The continuous line represents the experimental data and the broken line the theoretical result. For details of fit parameters see Table 1, columns headed S_1^*, S_2^*, S_3^*; and Table 2, columns headed S_1^* egta, S_2^* egta, S_3^* egta.

with high concentrations of NaCl in the present study show changes in the XANES and EXAFS modulations for the S_1^* state that do not markedly differ on formation of the S_3^* state suggesting that significant effects occur in S_1. All three methods of salt treatment gave similar XANES and EXAFS data for a given S-state.

The Fourier transforms of the k^3-data reveal four peaks corresponding to shells of scatterers at $\approx$ 1.8, 2.7, 3.6 and 4.0–5.0 Å respectively. There is an apparent reduction in the intensity of the Fourier features at $>$ 2 Å for the S_1^* NaCl-treated samples relative to the untreated PS II preparation, indicative of differences in degree of order or structure between the two types of sample. The NaCl-treated samples show a more complicated Fourier transform than the untreated S_1 sample. For both types of sample, ± EGTA, the intensity of the 1.8 Å Fourier peak increases with increasing S-state. Such a change can be explained by an oxidation state increase for each of the S-state transitions, resulting in a narrower range of Mn-O/N bond lengths.

Simulations of scatterers located by the first Fourier transform peak

Initial curve fitting was carried out using Fourier filtered data and Fourier limits as indicated in Figs. 7,

Table 1
Fits to k^3-weighted Fourier filtered EXAFS data for NaCl-treated samples

	S_1^*	Mn	Cl	S_2^*	Mn	Cl	S_3^*	Mn
r1	1.85	1.85	1.86	1.86	1.86	1.88	1.86	1.86
r2	–	–	2.46	–	–	2.44	–	–
r3	2.68	2.68	2.68	2.69	2.70	2.70	2.71	2.72
r4	–	2.98	–	–	3.06	–	–	3.03
r5	3.65	3.65	3.65	3.7	3.7	3.7	3.65	3.65
$\alpha 1$	0.030	0.030	0.030	0.021	0.022	0.020	0.018	0.022
$\alpha 2$	–	–	0.009	–	–	0.024	–	–
$\alpha 3$	0.006	0.005	0.008	0.008	0.009	0.010	0.009	0.009
$\alpha 4$	–	0.039	–	–	0.022	–	–	0.022
$\alpha 5$	0.012	0.012	0.011	0.016	0.016	0.017	0.019	0.018
E_0	27.3	27.3	25.5	25.7	25.9	23.2	26.0	25.9
N_1	14.2	14.2	14.2	14.4	14.4	14.4	14.3	14.3
p	7	9	9	7	9	9	7	9
FI · 10^3	0.486	0.397	0.301	0.602	0.431	0.366	0.422	0.250
R	21.05	18.98	15.71	24.97	22.08	19.22	20.81	15.64
$\epsilon_v^2 \cdot 10^6$	6.16	6.96	5.29	7.58	7.43	6.31	5.28	4.29

The fits shown are the basic model given in the text with oxygen ligation in the first shell and a single manganese distance in the second and third shell; 5 O, 1 Mn, 1 Mn (labelled S_1^*, S_2^*, S_3^*). Additional fits to include another manganese shell (labelled Mn) 5 O, 1 Mn, 1 Mn, 1 Mn, or chloride (Cl^-) ligation 5 O, 1 Cl^-, 1 Mn, 1 Mn are also shown for each S-state. Other details and an explanation of the statistics are given in Section 2.

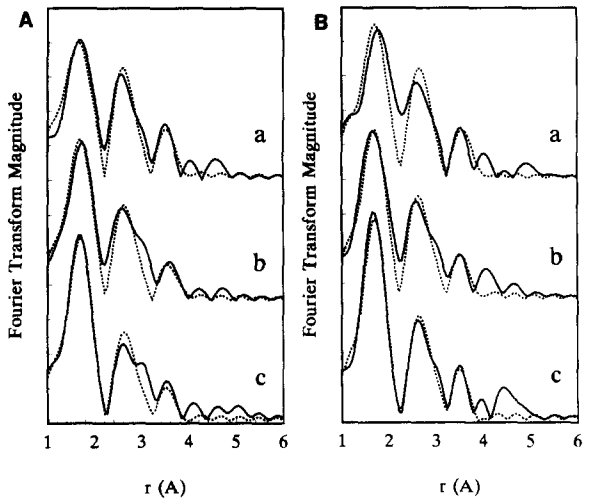

Fig. 8. Three shell fits to the k^3-weighted Fourier transforms of EXAFS spectra from (A) NaCl-treated samples and (B) NaCl-EGTA treated samples. Samples were in the (a) S_1^*, (b) S_2^* and (c) S_3^* states. The Fourier window was 0.7–4.5 Å, uncorrected for phase. The continuous line represents the experimental data and the broken line the theoretical result. For details of fit parameters see Tables 1 and 2.

Table 3
Fits to k^3-weighted Fourier filtered EXAFS data for untreated PS II membranes in S_1 and calcium-depleted samples with or without the 17 and 23 kDa extrinsic polypeptides (labelled + ex and − ex)

	S_1^*-Ca	S_1^*-Ca −ex	S_1 + ex
r1	1.83	1.82	1.85
r2	2.70	2.69	2.69
r3	3.02	2.96	–
r4	3.7	3.6	3.7
α1	0.022	0.023	0.027
α2	0.009	0.012	0.004
α3	0.022	0.017	–
α4	0.019	0.011	0.009
E_0	26.5	29.2	28.4
N_I	14.6	14.3	14.4
p	9	9	7
FI·10^3	1.16	1.60	1.89
R	38.85	48.61	44.26
$\epsilon_v^2 \cdot 10^6$	14.09	18.39	19.84

Fits comprise 4 O, 1 Mn, 1 Mn for calcium-depleted samples and 6 O 1 Mn, 1 Mn, 1 Ca for untreated PS II membranes. Note that if Ca is replaced by Mn, the distances are 0.03–0.05 Å shorter. Other parameters as given in Table 1 and Section 2.

8 and Tables 1–3. As the manganese coordination is presently unknown and EXAFS cannot usually distinguish between backscattering atoms of similar atomic number, the data were fitted with models containing only oxygen coordination. Ligation by nitrogen or oxygen is difficult to resolve. The distances obtained with fits using nitrogen ligands (not shown) are only slightly longer, ≈ 0.03 Å, than found using oxygen coordination.

On fitting a single shell of oxygens to the raw data, at the distance indicated by the first Fourier transform peak, a best fit distance of 1.84–1.89 Å and coordination number of 4.0–6.0 were obtained for all the sample types. A single shell fit was adequate for the S_2^* and S_3^* state NaCl-treated samples, with and without EGTA. The presence of additional shells of scatterers at > 2.0 Å was indicated by the poor fit to both the modulations and Fourier transform, as illustrated in the Fourier filtered data for the S_1^* state in samples containing EGTA shown in Fig. 8. The fit showed no improvement in statistics for two shell models containing just oxygen, Tables 1–3. It should be noted that it is often found that the fitting of a single wave introduces

Table 2
Fits to k^3-weighted Fourier filtered EXAFS data for NaCl-EGTA treated samples

	S_1^*egta	Mn	Cl	S_2^*egta	Mn	Cl	S_3^*egta	Mn
r1	1.88	1.88	1.90	1.85	1.85	1.87	1.85	1.85
r2	–	–	2.52	–	–	2.50	–	–
r3	2.71	2.72	2.70	2.70	2.70	2.70	2.71	2.71
r4	–	2.97	–	–	3.03	–	–	2.99
r5	3.65	3.65	3.65	3.65	3.65	3.65	3.7	3.7
α1	0.021	0.021	0.021	0.020	0.020	0.020	0.016	0.016
α2	–	–	0.009	–	–	0.024	–	–
α3	0.005	0.004	0.008	0.006	0.007	0.007	0.006	0.005
α4	–	0.024	–	–	0.035	–	–	0.038
α5	0.011	0.011	0.010	0.014	0.014	0.014	0.009	0.009
E_0	24.6	24.7	22.4	24.1	26.3	21.6	24.7	24.5
N_I	14.1	14.1	14.1	14.2	14.2	14.2	14.4	14.4
p	7	9	9	7	9	9	7	9
FI · 10^3	0.852	0.668	0.328	0.524	0.448	0.434	0.372	0.334
R	30.8	26.4	18.89	24.14	22.70	21.55	20.57	19.23
$\epsilon_v^2 \cdot 10^6$	11.05	12.06	5.94	6.60	7.78	7.59	4.64	5.69

The fits shown are the basic model given in the text and Table 1 (labelled S_1^*, S_2^*, S_3^*). Additional fits to include another manganese shell (labelled Mn) or chloride (Cl^-) ligation are also shown for each S-state. Other values are explained in Table 1 and Section 2.

systematic errors in both the average bond lengths and coordination numbers [43]. If a shell of chlorine atoms is introduced a much improved fit is obtained with 0.25–1.0 chlorine at 2.4–2.5 Å with a reduction in FI, R and ϵ_v^2 of 30–60% for the Fourier filtered data, Tables 1 and 2. This was not the case for samples retaining all the extrinsic polypeptides including untreated S_1 and S_2 samples where oxygen shells adequately fit the data, and we are unable to arrive at fits including chlorine that were significantly better than the split oxygen shell models. For the calcium-depleted samples retaining extrinsic polypeptides, the best fit distances for single shell fits are the same as in untreated PS II membranes and HTG PS II, for which the range 1.83–1.86 Å is obtained for fits of oxygen scatterers to the first shell [26].

Coordination numbers for the first shell of 4–6 and short distance of the oxygen shell, Mn-O 1.84–1.89 Å, probably reflect disorder in the expected longer oxygen shells of the non-bridging ligands, giving rise to destructive interference among the scattered photoelectrons, rather than indicating four or five coordinate manganese. Four coordinate manganese can be ruled out as the expected intensity of the pre-edge feature would be larger than observed. The presence of five coordinate manganese cannot be excluded. For the NaCl-treated samples the best fit distances for the single shell fits are in the same range as untreated PS II membranes, 1.83–1.86 Å. The presence of a short Mn–O bond demonstrates the retention of a short oxo-bridge in the NaCl-treated samples, consistent with oxo-bridged binuclear manganese centres in untreated samples.

Simulation of the scatterers located by the second Fourier transform peak

For the distance corresponding to the second Fourier transform peak a model incorporating 1.0 manganese at 2.69–2.71 Å did not adequately fit the data for all calcium depletion treatments indicating the presence of further shells of scatterers suggested by the pronounced shoulder at ≈ 3.0 Å in the Fourier transforms. Attempts to fit two shells of scatterers at this distance resulted in models with an additional shell of manganese atoms at 3.0 Å for all the samples. The fits with a second manganese shell were not statistically significantly better compared to fits with calcium, chlorine, oxygen or carbon shells, irrespective of whether wide or narrow filter limits were used to isolate the peak or whether smoothed or the raw data was modelled.

Several authors have reported difficulty obtaining unique fits to the second coordination sphere of dinuclear transition metal complexes [44,45]. This situation can arise because the second shell generally contains a contribution from carbon, nitrogen and oxygen scatterers at distances near that of the metal/metal separation. Interference among these shells can alter the shape of the backscattering envelope from these low Z atoms to be similar to that of a metal. The backscattering envelope from a manganese scatterer should normally maximise at higher k values than that of low Z scatterers such as carbon, oxygen or nitrogen. Mutations of the carboxylate, histidine and tyrosine residues on the luminal side of D1 have produced mutations that abolish or impair photoautotrophic growth and water oxidation. These may be considered as potential manganese ligands. One possibility is that the features at 3.0 and 4–5 Å arise from multiple scattering interactions of ring systems, histidine or tyrosine ligands. ESEEM and ENDOR spectra indicate that the number of histidine ligands is small, perhaps one or two per four manganese [1–4,40,46]. We suggest that the intensity of the 3.0 Å shell would argue against low Z scatterers such as carbon, oxygen or nitrogen being responsible though we cannot rule them out. If the shell at 3.0 Å arises from manganese, then the apparent shift in second sphere observed coordination number is within the error for this measurement and changes from 1.0 ± 0.5 for untreated PS II membranes to 1.5 ± 1.0 for NaCl-treated samples.

On S-state advance the size of the shoulder at 3.0 Å increases, though the distances modelled remain the same, within experimental errors. No bond length changes were observed despite an apparent increase in the Mn K-edge, the observed changes in both the pre-edge feature and the intensity of the first Fourier peak which together signify manganese oxidations for each of these steps.

Simulation of the scatterers located by the third Fourier transform peak

As reported in an earlier study [26], we do not observe scatterers at 3.3 Å reported for studies (reviewed in [4]), instead all our samples have scatterers at about 3.6 Å. The difference is related to modelling approaches rather than sample differences. We employ ab initio phase shifts and an adjustable reference energy or inner potential, E_0, to correct for imperfections in the theory used to calculate the ab initio phase shifts [26,38]. If E_0 is set to zero, the raw data and Fourier transforms of an untreated S_1 or S_2 sample are as reported by other authors [4,23–25,27,28,47]. The phase shifts used have been tested on model compounds [26] and shown to adequately reproduce crystallographic distances. Other studies have used phase shifts derived from model compounds, rather than calculated theoretically, and these were tested on well characterised compounds. However, this approach also requires the use of theoretical phase shifts for the manganese interactions as no suitable model compounds are available. The difference in approaches seems to have the great-

est effect on the third peak in Fourier tranform at 3.3/3.6 Å.

The interpretation of the scatterers responsible for the 3.6 Å distance is problematic, as might be expected for a polynuclear manganese complex for which several types of scatterer could contribute to shells further from the manganese. Inclusion of a shell of scatterers at ≈ 3.6 Å resulted in a ≈ 10–15% reduction in the fit index for models including Mn, Ca, C or Cl for the raw data for the PS II membranes (not shown). Unfortunately the present data did not allow the generation of models that significantly favour one of manganese or calcium as the scatterer at 3.6 Å. As discussed for the fitting of the second shell, it might be reasonable to assume that the 3.6 Å peak also results from the interference of two or more shells of low Z scatterers resulting in a backscattering envelope which resembles that of a metal. However, fits employing low Z atoms at 3.6 Å resulted in models with negative Debye-Waller factors, a physical impossibility, and so were discounted. Alternatively the 3.6 Å interaction could be the result of multiple scattering pathways from ligands such as histidine or tyrosine, and the identification of calcium as the scatterer at this distance with single scattering theory would then just be a fortuitous occurrence. Another possibility is that the third Fourier transform peak has contributions from more than one kind of scatterer. Unfortunately the number of independent points for the third Fourier peak, 3–4, is not enough to enable the fitting of a split shell to this peak for which > 4 independent points would be required.

The relative intensity of the Fourier peak at 3.6 Å is reduced for the NaCl-treated samples compared to the untreated PS II S_1 sample. Although the difference can be accounted for in terms of increased disorder, reflected in increased Debye-Waller factors if the coordination number remains constant, the simplest explanation would be a reduction in the scattering power through a lower coordination number.

3.4. Pulsed EPR

Changes occurring in the manganese complex on S-state advancement in NaCl-treated samples were also examined indirectly using the effect of the complex on the relaxation time of the $Y_D^{\cdot}$ radical. The relaxation time of the $Y_D^{\cdot}$ radical was investigated by pulsed EPR spectroscopy of samples in the S_1^*, S_2^* and S_3^* states. Care was taken to monitor the iron-semiquinone and cytochrome *b*-559 EPR signals to ensure that differences were not due to changes in the non-haem and/or cytochrome iron redox states, which may have affected the T_1 times.

Initially the repetition rate recovery method was used to measure the electron spin lattice relaxation times and the results obtained indicated that the relaxation times decrease as a function of increasing S-state. The drawback of the repetition rate recovery method for the measurement of electron spin-lattice relaxation times is that the value of the T_1 so obtained is contaminated by the effects of spectral diffusion. For an inhomogeneously broadened EPR line, spectral diffusion has the effect of spreading the saturation from spins that are in resonance to non-resonant spins. This enhances the observed electron spin lattice relaxation rate which has two rate components, one due to the intrinsic electron spin lattice relaxation rate and one due to spectral diffusion. In order to minimise the effects of spectral diffusion one can apply a long saturating pulse which has the effect of burning a sufficiently large hole in the signal so that spectral diffusion cannot relax the electron at the field of interest. Therefore, the effect of a long saturating pulse has the two-fold function of saturating the signal and removing the effects of spectral diffusion. This was confirmed by studies using saturating pulses of different lengths.

The results of five saturation recovery experiments on five different sample preparations were averaged. The relaxation times obtained from saturation recovery are longer than those using the repetition rate recovery method indicating that contamination from spectral diffusion has been removed. However the trend observed previously is maintained, i.e. that the relaxation times decrease on the transition from S_1^* to S_2^*, and from S_2^* to S_3^*. A representative fit is shown in Fig. 9.

Previous studies of $Y_D^{\cdot}$ saturation recovery kinetics have determined nonexponential decay rates (e.g., [34]). Nonexponential rates for $Y_D^{\cdot}$ relaxation recovery have been attributed to the different components of relax-

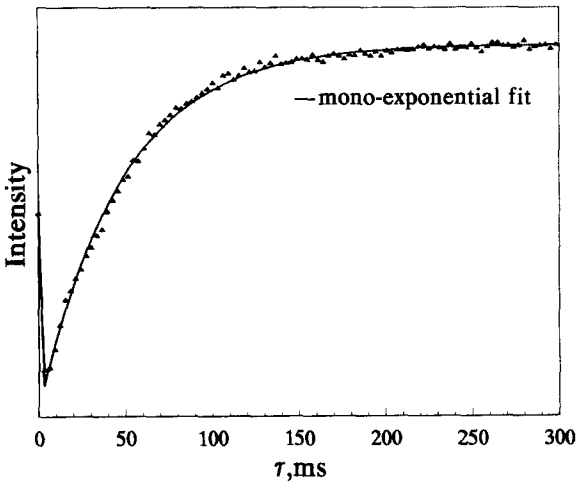

Fig. 9. Saturation recovery transients observed at 4 K for the stable tyrosine radical $Y_D^{\cdot}$ in NaCl-EGTA-treated PS II. An example of a single exponential fit (solid line) to experimental data is shown. The vertical scale is arbitrary. The length of the saturating pulse was 2000 ns.

ation from scalar and dipolar exchange interactions. The dipolar exchange interactions were proposed to occur by exchange coupling to the non-heme iron and the manganese cluster, both present in intact PS II [31–4,48,49]. We do observe an influence of both the manganese cluster and the non-heme iron on the relaxation transients of $Y_D^{\cdot}$.

A monoexponential fitting (Fig. 9) proved adequate to fit the data and we could not deconvolute the data into two distributions of T_1's. However, in a frozen glassy sample there is a random distribution of orientations which can contribute to the observed saturation recovery transient. Therefore the observed saturation recovery transient will be the sum of many different exponential recovery rates. If one assumes a purely dipolar relaxation mechanism this is described in [34] by

$$I(t) = 1 - N\int_0^{\pi} \sin\theta[e^{-(X)t}]d\theta$$

where

$$X = R_{1\theta} = R_{1D}(1 - 3\cos^2\theta)^2$$

and $I(t)$ is the intensity of the saturation recovery transient as a function of time, N is an adjustable scaling factor, θ is the angle between the magnetic field and the interspin vector with R_{1D} being the inverse of T_{1D}, the dipolar relaxation time. The experimental saturation recovery transients were therefore also fitted using non linear least squares fitting according to this model with 30 increments between 0 and π. Examples of these fits are shown in Fig. 10. The results are compared to the results from the pseudomonoexponential fitting and displayed graphically in Fig. 11. A

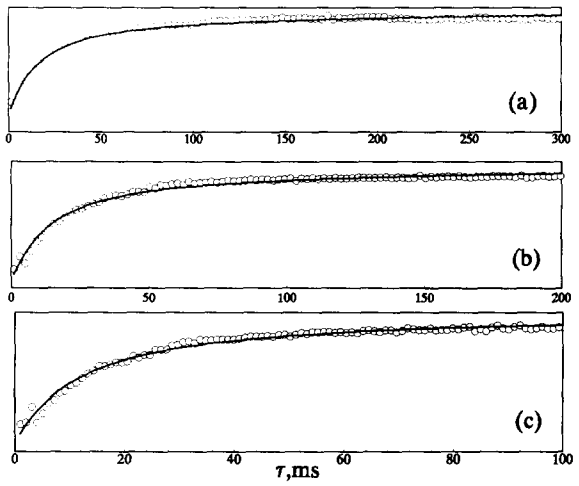

Fig. 10. Examples of typical fits to the dipolar powder average model for the relaxation of $Y_D^{\cdot}$ in various modified S-states. NaCl-EGTA-treated samples. The signal intensity scale is arbitrary. (a) S_1^*, (b) S_2^*, (c) S_3^*. The length of the saturating pulse was 2000 ns. Further details are given in the text.

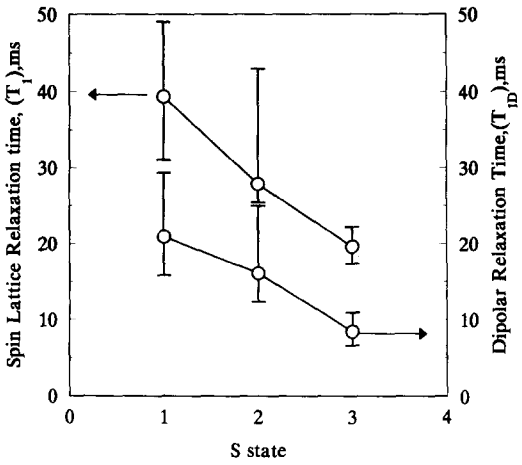

Fig. 11. Plots of spin lattice and dipolar relaxation times for tyrosine radical $Y_D^{\cdot}$, in samples in different modified S-states. NaCl-EGTA-treated samples. Rates calculated as given in the text. Each circle shows the average of 20 measurements across the $Y_D^{\cdot}$ spectrum using four preparations. The arrows indicate the scales to which each plot belongs. The bars show the range of the data, i.e., the maximum and minimum values obtained across the $Y_D^{\cdot}$ spectrum. The actual values (in ms) are T_1: S_1^* 39.35 (range 31–49), S_2^* 27.84 (25.42–43), S_3^* 19.6 (17.34–22.2); T_{1D}: S_1^* 20.9 (15.8–29.3), S_2^* 16.09 (12.32–24.97), S_3^* 8.43 (6.6–10.94).

decrease of relaxation time with increasing S-state was again observed.

4. Discussion

The S_1 state in native samples has been proposed to have a $Mn_4(III_4)$ or $Mn_4(III_2, IV_2)$ oxidation state, with the former favoured by photoactivation experiments and some EPR simulations of the various S_2 state EPR signals, while the latter option is most favoured by XAS studies (see [1–4]). XAS studies of the Mn K-edge have shown a decrease in edge energy for S_1^* on NaCl treatment consistent with either a conformational change or a manganese reduction [28,29]. That no new EPR signal is observed in the NaCl-treated/calcium-depleted S_1^* state, while a signal forms on a one electron oxidation to S_2^*, favours a conformational rather than a redox change for the S_1^* NaCl-treated sample relative to the untreated S_1 state.

Changes in the overall oxidation state of the manganese cluster on S-state advancement should be reflected by changes in T_1 times for the $Y_D^{\cdot}$ radical. The electron spin relaxation power of the manganese oxidation states follows the order Mn(II) ≫ Mn(IV) > Mn(III). As the proportion of Mn(IV) increases with S-state, the T_1 times should decrease. From Fig. 11, it can be seen that the T_1 times decrease for the transitions $S_1^* \rightarrow S_2^*$ and $S_2^* \rightarrow S_3^*$ studied in NaCl-treated samples. The results presented infer that the man-

ganese complex in PS II is oxidised on the S_2^* to S_3^* transition in samples for which the S_3 to S_0 transition is blocked. This result agrees with XANES studies of the Mn K-edge in untreated PS II membranes [50] and in calcium-depleted and salt-treated PS II [29] which indicate oxidation of manganese on the S_2 to S_3 transition (or $S_2^* \rightarrow S_3^*$). However oxidation of an amino acid close to the manganese cluster could affect the T_1 time because of the resulting interaction.

It was previously thought that no manganese oxidation occurred on the S_2 to S_3 transition in native and calcium-depleted membranes. As a result the S3 EPR signal was attributed to the oxidation of histidine or $Y_Z^{\cdot}$ [10,22], which weakly interacts with the manganese cluster to give rise to the S3 EPR signal. As the simplest explanation of the data is now that the manganese complex can be oxidised, there may no longer be any need to invoke a radical oxidation in S_3^*. This would leave the manganese complex as the centre responsible for the S3 signal. This is however difficult to reconcile with the EPR properties. Alternatively the explanation could be a radical interacting with the manganese cluster having the same oxidation state as in the S_2 state, i.e. S_2^*, but this would occur in only a small fraction of centres in order to explain the Mn K-edge data for the $S_2^* \rightarrow S_3^*$ transition. Support for this explanation comes from quantitation studies of the S3 EPR signal which suggest it occurs in $< 25\%$ of centres [51]. Zimmermann et al. [52] obtained higher yields in their quantitation study of the S3 signal. However their data is affected by saturation effects arising from the repetition rate used in their experiments (i.e. the waiting time between pulse trains was too short). A third explanation accounting for XANES and EPR data would be that the radical is a manganese ligand but to the the postulated even valence Mn pair (Mn_2(III, III) or Mn_2(IV, IV)) and not the Mn_2(III, IV) pair which is largely responsible for the EPR properties of the S_2 state.

Calcium depletion by NaCl treatment in the presence of EGTA results in the formation of an altered S_2 multiline and a block in S-state advancement past S_3 (see [1,3] for reviews). The formation of an altered multiline in samples containing EGTA implies some change in ligand or ligand geometry, altering the exchange coupling between manganese centres, which should be detectable by XAS. From curve fitting to the first shell of scatterers, there is no dramatic change in either the number or average distance of the bridging ligands on NaCl treatment, though changes may be too subtle to detect in the present study. The small changes in the edge region caused by EGTA, thought to bind at or near to the manganese complex, are difficult to quantify.

It is interesting that the samples without the 17 and 23 kDa extrinsic polypeptides can be modelled with a small chlorine contribution at ≈ 2.4 Å. Though such models are speculative, they might be explained by changes in solvent access or ligands after removal of the 17 and 23 kDa extrinsic polypeptides. Support for such an observation has recently been provided by thermoluminescence studies [53,54]. Thermoluminescence of samples treated with NaCl, as in the present study, or with pH 3 citrate show differences depending on the binding of the 23 kDa protein and chelators. The changes have been interpreted as showing that the 23 kDa protein regulates the structure and function of the manganese cluster. Changes could be due to ligands provided by the extrinsic polypeptide or more likely from conformational changes to the reaction centre manganese polypeptide structure induced by peptide binding [53,54]. The changes on removal of the 17 and 23 kDa extrinsic polypeptides are small compared to the effect of the NaCl treatment. Such an observation agrees with previous studies which did not find significant differences between PS II samples depleted of the 17, 23 and 33 kDa extrinsic polypeptides and untreated samples [55].

By far the biggest effect detected as a result of NaCl treatment is on the 2.7 Å Fourier feature which is split into two shells, at 2.7 Å and 3.0 Å. We can postulate that both shells are due to manganese interactions rather than low Z scatterers which implies that there are at least two dimeric manganese structural motifs present. Presumably in the untreated sample both have a Mn-Mn distance of 2.7 Å, whereas in the 'NaCl treated/calcium-depleted' type sample a structural modification has occurred in one of the dimers, perhaps the loss of an oxo bridge, or in a ligand linking the dimers, e.g. a carboxylate shift. Such a structural change would also explain the reduction in the edge energy of a calcium-depleted sample in S_1^* relative to the intact PS II membranes in S_1, without the need for manganese reduction [28,29].

The location of the calcium site required for oxygen evolution is unknown. The identification of features in the EXAFS at 3.3/3.6 Å and 4.3 Å have led to proposals that calcium might be found at one of these distances (see [1–4]). Our results do not provide clear evidence for an interaction at 4–5 Å, so we will restrict discussion to the 3.3/3.6 Å interaction. In the present study, depletion was carried out by treatment with a high concentration of sodium cations, a competitive inhibitor of oxygen evolution [6], which should bind at the calcium site. As the size and coordination requirements of calcium and sodium differ, the distance corresponding to a manganese-calcium/sodium interaction might be expected to change. Following calcium depletion by NaCl treatment there appears to be no change in the distance for the 3.3/3.6 Å interaction attributed to variously Mn, C, Ca or combinations of these compared to untreated samples. However, the intensity of

this peak is reduced compared to the untreated sample. Sodium has lower X-ray scattering power than calcium so the intensity of the Fourier peak at 3.3/3.6 Å, if mainly due to calcium in untreated samples, would be decreased in NaCl-treated/calcium-depleted samples due to sodium replacing calcium. Possibly the occupancy of the calcium site by sodium results in greater disorder as reflected in larger Debye-Waller factors. To confirm a calcium interaction at 3.3/3.6 Å, protein conformational changes close to the cluster must be ruled out by further experiments. If calcium is not located close to the manganese complex then the role of calcium could be structural, maintaining the correct reaction centre conformation for the ligands to the manganese complex to exert a role in influencing the complex redox potential.

An appropriate model for the manganese complex based on the information gained here and combined with that from EPR and previous reports would be a structure comprising two or more manganese oxo-bridged dimeric units. The interdimer distance may be 3.3/3.6 Å, roughly perpendicular to the membrane in accordance with XAS studies of oriented membranes (see [4]). However if this represents a Mn-Ca distance, then the interdimer distance would be larger. For the native state each dimer would have a Mn-Mn separation of 2.7 Å, giving rise to S_2 a 16–19 line multiline, with probable oxidation state $Mn_4(III,IV_3)$ for the tetramer or 'dimer of dimers'. The number of oxo-bridging ligands could vary in an S-state dependent manner. In the calcium-depleted/NaCl-treated samples one of the dimer Mn-Mn separations becomes 3.0 Å, resulting in reduced exchange coupling and an S_2^* state with a 32 line 'altered multiline'. On change of S-states, from S_1^* to S_3^*, we do not see significant changes in the EXAFS except those that may be due to oxidation of manganese, i.e., no major structural rearrangements occur.

Acknowledgements

We wish to thank Dr Samar Hasnain, Dr Richard Strange, Dr Margaret Neu, Menno Oversluizen and Lorrie Murphy at the SRS Daresbury for their help. We also wish to thank Dr Stephen Rigby and Dr Sandra Turconi for helpful comments and discussion. We acknowledge financial assistance from the U.K. Science and Engineering Research Council.

References

[1] Debus, R.J. (1992) Biochim. Biophys. Acta 1102, 269–352.
[2] Renger, G. (1992) in The Photosystems: Structure, Function and Molecular Biology (Barber, J., ed.), Chapter 3, pp. 45–99, Elsevier, Amsterdam.
[3] Rutherford, A.W., Zimmermann, J.-L. and Boussac, A. (1992) in The Photosystems: Structure, Function and Molecular Biology (Barber, J., ed.), Chapter 5, pp. 179–229, Elsevier, Amsterdam.
[4] Yachandra, V.K., DeRose, V.J., Latimer, M.J., Mukerji, I., Sauer, K. and Klein, M. (1993) Science 260, 675–679.
[5] Coleman, W.J. (1990) Photosynthesis Res. 23, 1–27.
[6] Yocum, C.F. (1991) Biochim. Biophys. Acta 1059, 1–15.
[7] Dekker, J.P., Ghanotakis, P.F., Plijter, J.J., Van Gorkum, H.J. and Babcock, G.T. (1984) Biochim. Biophys. Acta 767, 515–523.
[8] Cole, J. and Sauer, K. (1987) Biochim. Biophys. Acta 891, 40–48.
[9] Kalosaka, K., Beck, W.F., Brudvig, G. and Cheniae, G. (1990) in Current Research in Photosynthesis, vol. 1 (Baltscheffsky, M., ed.), pp. 721–724, Kluwer, Dordrecht.
[10] Hallahan, B.J., Nugent, J.H.A., Warden, J.T. and Evans, M.C.W. (1992) Biochemistry 31, 4562–4573.
[11] Weber, A.N. and Gray, J.C. (1989) FEBS Lett. 249, 79–82.
[12] Han, K.-C. and Katoh, S. (1992) in Research in Photosynthesis, Vol. II, pp. 365–368, Kluwer, Dordrecht.
[13] Boussac, A. and Rutherford A.W. (1988) Biochemistry 27, 3476–3483.
[14] Ono, T. and Inoue, Y. (1988) FEBS Lett. 227, 147–152.
[15] Boussac, A., Zimmermann, J.-L. and Rutherford, A.W. (1989) Biochemistry 28, 8984–8989.
[16] Sivaraja, M., Tso, J. and Dismukes, G.C. (1989) Biochemistry 28, 9459–9464.
[17] Ono, T. and Inoue, Y. (1990) Biochim. Biophys. Acta 1020, 269–277.
[18] Ghanotakis, D.F., Babcock, G.T. and Yocum, C.F. (1984) FEBS Lett. 167, 127–130.
[19] Dismukes, G.C. and Siderer, Y. (1980) FEBS Lett. 121, 78–80.
[20] Boussac, A., Zimmermann, J.-L. and Rutherford, A.W. (1990) FEBS Lett. 277, 69–74.
[21] Boussac, A., Maison-Peteri, B., Vernotte, C. and Etienne, A.-L. (1985) Biochim. Biophys. Acta 808, 225–230.
[22] Boussac, A., Zimmermann, J.-L., Rutherford, A.W. and Lavergne, J. (1990) Nature 347, 303–306.
[23] Goodin, D.B., Yachandra, V.K., Britt, R.D., Sauer, K. and Klein, M.P. (1984) Biochim. Biophys. Acta 767, 209–216.
[24] Yachandra, V.K., Guiles, R.D., McDermott, A.E., Britt, R.D., Dexheimer, S.L., Sauer, K. and Klein, M.P. (1986) Biochim. Biophys. Acta 850, 324–332.
[25] Kusunoki, M., Ono, T., Matsushita, T., Oyanagi, H. and Inoue, Y. (1990) J. Biochem. 108, 560–567.
[26] MacLachlan, D.J., Hallahan, B.J., Ruffle, S.V., Nugent, J.H.A., Evans, M.C.W., Strange, R.W. and Hasnain, S.S. (1992) Biochem. J. 285, 569–576.
[27] Guiles, R.D., Zimmermann, J.-L., McDermott, A.E., Yachandra, V.K., Cole, J.L., Dexheimer, S.L., Britt, R.D., Weighardt, K., Bossek, U., Sauer, K. and Klein, M.P. (1990) Biochemistry 29, 471–496.
[28] Ono, T., Kusunoki, M., Matsushita, T., Oyanagi, H. and Inoue, Y. (1991) Biochemistry 30, 6836–6841.
[29] MacLachlan, D.J., Nugent, J.H.A. and Evans, M.C.W. (1994) Biochim. Biophys. Acta 1185, 103–111.
[30] Enami, I., Kamino, K., Shen, J.R., Satoh, K. and Katoh, S. (1989) Biochim. Biophys. Acta 977, 33–39.
[31] de Groot, A., Plitjer, J.J., Evelo, R., Babcock, G.T. and Hoff, A.J. (1986) Biochim. Biophys. Acta 848, 8–15.
[32] Styring, S.A. and Rutherford, A.W. (1988) Biochemistry 27, 4915–4923.
[33] Evelo, R.G., Styring, S.A., Rutherford, A.W. and Hoff, A.J. (1989) Biochim. Biophys. Acta 973, 428–442.
[34] Hirsh, D.J., Beck, W.F., Innes, J.B. and Brudvig, G.W. (1992) Biochemistry 31, 532–541.

[35] Berthold, D.A., Babcock, G.T. and Yocum, C.F. (1981) FEBS Lett. 134, 231–234.
[36] Ford, R.C. and Evans, M.C.W. (1983) FEBS Lett. 160, 159–163.
[37] Maclachlan, D.J. and Nugent, J.H.A. (1993) Biochemistry 32, 9772–9780.
[38] Gurman, S.J., Binsted, N. and Ross, I. (1984) J. Phys. C. Solid State Phys. 17, 143–151.
[39] Gurman, S.J. and Pendry, J.B. (1976) Solid State Commun. 28, 287–290.
[40] Britt, R.D., Zimmermann, J.L., Sauer, K. and Klein, M.P. (1989) J. Am. Chem. Soc. 111, 3522–3532.
[41] Nugent, J.H.A., MacLachlan, D.J., Rigby, S.E.J. and Evans M.C.W. (1993) Photosynth. Res. 38, 341–346.
[42] MacLachlan, D.J., Nugent, J.H.A. and Evans, M.C.W. (1992) in Research in Photosynthesis (Murata, N., ed.), Vol II, pp. 373–380, Kluwer, Dordrecht.
[43] Scarrow, R.C., Maroney, M.J., Palmer, S.M., Que, L. Jr., Roe, A.L., Salowe, S.P. and Stubbe, J. (1987), J. Am. Chem. Soc. 109, 7857–7864.
[44] Scott, R.A. and Eidsness, M.K. (1988) Comments Inorg. Chem. 7, 235–267.
[45] DeWitt, J.G., Bentsen, J.G., Rosenzweig, A.C., Hedman, B., Green, J., Pilkington, S., Papaefthymiou, G.C., Dalton, H., Hodgson, K.O. and Lippard, S.J. (1991) J. Am. Chem. Soc., 113, 9219–9235.
[46] Tang, X.S., Sivaraja, M. and Dismukes, G.C. (1993) J. Am. Chem. Soc. 115, 2382–2389.
[47] Penner-Hahn, J.E., Fronko, R.M., Pecoraro, V.L., Yocum, C.F., Bretts, S.D. and Bowlby, N.R. (1990) J. Am. Chem. Soc. 112, 2549–2557.
[48] Beck, W.F., Innes, J.B. and Brudvig, G.W. (1990) in Current Research in Photosynthesis (Baltscheffsky, M., ed), Vol. I, pp. 817–820 Kluwer, Dordrecht.
[49] Bosch, M.K., Evelo, R.G., Styring, S., Rutherford, A.W. and Hoff, A.J. (1991) FEBS Lett. 292, 279–283.
[50] Ono, T., Noguchi, T., Inoue, Y., Kusunoki, M., Matsushita, T. and Oyanagi, H. (1992) Science 258, 1335–1337.
[51] Gilchrist, M.L., Lorigan, G.A. and Britt, R.D. (1992) in Research in Photosynthesis (Murata, N., ed.), Vol. II, pp. 317–320, Kluwer, Dordrecht.
[52] Zimmermann, J.-L., Boussac, A. and Rutherford, A.W. (1993) Biochemistry 32, 4831–4841.
[53] Ono, T., Izawa, S. and Inoue, Y. (1992) Biochemistry 31, 7648–7655.
[54] Homann, P.H. and Madabusi, L.V. (1993) Photosynth. Res. 35, 29–39.
[55] Cole, J., Yachandra, V.K., McDermott, A.E., Guiles, R.D., Britt, R.D., Dexheimer, S.L., Sauer, K. and Klein, M.P. (1987) Biochemistry, 26, 5967–5973.